

On the derivation of kernels for kernel-driven models of bidirectional reflectance

W. Wanner, X. Li, and A. H. Strahler

Center for Remote Sensing, Boston University, Boston, Massachusetts

Abstract. A new approximation to Ross' (1981) radiative transfer theory for small values of leaf area index (LAI) and two new approximations to Li and Strahler's (1992) geometric-optical mutual shadowing model are derived. These, together with Roujean et al.'s (1992) approximation to Ross' theory for large LAI and their geometric-optical model of rectangular protrusions, may be used for formulating semiempirical models of the bidirectional reflectance distribution function (BRDF) of the land surface through linear combinations. Because the functions superimposed depend only on viewing and illumination geometry, the BRDF models derived may be called kernel-driven; but Nilson and Kuusk's (1989) modified version of Walthall et al.'s (1985) model is an example of an empirical model that belongs to this same class. The linearity of kernel-driven models is advantageous to global BRDF and albedo processing needs in several respects, most notably analytical invertibility, making possible look-up table approaches to albedo calculation, accommodation of mixed pixel situations, and spatial scaling. The models discussed here are being proposed for BRDF/albedo processing for the moderate resolution imaging spectroradiometer (MODIS) sensor of NASA's Earth Observing System (EOS).

1. Introduction

Kernel-driven models for the bidirectional reflectance distribution function (BRDF) of vegetated land surfaces attempt to describe the BRDF as a linear superposition of a set of kernels that describe basic BRDF shapes. Coefficients or weights are chosen to adapt the sum of the kernels to the given case.

If the kernels are chosen to be a set of mathematical functions selected solely because their shape seems to be able to model BRDFs as they are actually observed, the model is purely empirical. There is no physical basis for such kernels beyond their description of BRDF-like shapes. One example for such a model is the modified Walthall model [Walthall et al., 1985; Nilson and Kuusk, 1989].

If the kernels chosen are derived from approximations of more-detailed physical models, where the approximations are made in order to deduce from the complex model a BRDF shape typical for that model, the model may be called semiempirical. Typically, semiempirical kernels are based either on one of several possible approximations to a radiative transfer scenario of light scattering in a horizontally homogeneous plant canopy or on one of several approximations feasible in a geometric-optical model of light scattering in forestlike canopies of distinct crown shapes. With a Lambertian term added, a kernel-driven semiempirical BRDF model thus consists typically of an isotropic term, a volume scat-

tering term and a geometric scattering term [Roujean et al., 1992].

Semiempirical kernels can be of two types. First, they may contain only geometric terms but no physical parameters. The complete model then is linear and may be scaled to arbitrary spatial resolutions even for mixed scenes; neglecting adjacency effects, the weights of the kernels will be linear functions of the areal proportions of the subpixel weights. The so-called Ross kernels, approximations to Ross' [1981] radiative transfer theory in plant canopies, belong to this class, as does the so-called Roujean geometric-optical kernel [Roujean et al., 1992]. In the second case, kernels contain one or very few physical parameters and thus, instead of having one kernel, one is provided with a family of kernels depending on these parameters. The geometric-optical Li kernels [Strahler et al., 1994] belong to this type. An example for a semiempirical model that is nonlinear is the three-parameter model by Rahman et al. [1993].

This paper will first outline the role linear kernel-driven models may play in applicational BRDF modeling. Then expressions for two volume-scattering kernels, for thin and for thick canopies, will be given, where the approximation for the thin canopy is derived here for the first time. Following that, three surface-scattering kernels, the Roujean kernel and two Li kernels for dense and sparse stands of objects, will be presented, where the latter two, based on the Li-Strahler geometric optical mutual shadowing model, will also be derived here for the first time. Finally, the shapes of the kernels and their possible combinations will be discussed.

The performance of these kernels and the BRDF models derived from them will be discussed separately in a forthcoming paper, where they are applied extensively to measured data for different land cover types.

Copyright 1995 by the American Geophysical Union.

Paper number 95JD02371.
0148-0227/95/95JD-02371\$05.00

2. Applicational Context

2.1. Need for BRDF Analysis

Besides the spatial, temporal, and spectral content, the variation of pixel reflectance with viewing and illumination angle is a fourth potential source of information in remotely sensed data acquired at multiple angles [e.g., *Gerstl and Simmer*, 1986; *Pinty and Verstraete*, 1991; *Strahler*, 1994]. It also is the least explored of these sources of information.

Among the existing sensors some, like those on Landsat, provide views that are always close to nadir and, in a Sun-synchronous orbit, do not provide much angular information. Others, most notably the advanced very high resolution radiometers (AVHRR), have a very large field of view (e.g., 110° across track for AVHRR), introducing angular variations across each image. The need for taking BRDF effects into account in AVHRR data analysis, for example in land cover classification, is increasingly being recognized [*Li and Wu*, 1994; *Cihlar et al.*, 1994; *Gutman*, 1994; *Moody and Strahler*, 1994]. Recently, the along track scanning radiometer ATSR-2 has become operational, also providing some angular sampling.

Future sensors are more promising, and BRDF is among the products to be derived from these sensors [e.g., *Strahler et al.*, 1995; *Wanner et al.*, 1995]. POLDER (polarization and directionality of the Earth's reflectance) will have a field of view of 84° along track and 102° cross track, making it well suited for BRDF studies at coarse spatial resolution (several kilometers). Among the Earth Observing System (EOS) instruments, moderate resolution imaging spectroradiometer (MODIS) and multi-angle imaging spectro-radiometer (MISR) data may be combined over a given time period to provide cross-track and along-track scans of the BRDF of a pixel at the 1-km scale. For a discussion of existing and future sensors with respect to their ability to sample surface BRDFs, and for references on these sensors, refer to the comprehensive overview by *Barnsley et al.* [1994].

Three major goals are pursued by deriving and investigating the BRDF of the land surface. First, as indicated, there is a need to take angular effects in remotely sensed data into account when comparing the reflectances of pixels acquired at different viewing and/or illumination geometries. For example, it may be necessary to normalize multiangular data to a standard geometric situation (e.g., nadir view). This requires knowledge of the BRDF. Furthermore, one would like to extrapolate existing observations to angular ranges where no observations were made or can be made (e.g., nadir illumination).

Second, one would like to routinely derive precise albedo from remotely sensed data. Little is known about global albedo patterns and their seasonal change that is not based on estimates made from land cover and soil type. Global and mesoscale climate modelers are likely to require time series of global albedo in the future in order to better define their lower boundaries, which will more and more be biosphere models in their own right. Since albedo may be derived from BRDF, providing this information requires repeated observation and analysis of global BRDF patterns, about which not much is currently known.

Third, by inverting physical or semiempirical BRDF models for their parameters, some information about the surface may potentially be inferred. The angular variation of the observed reflectance contains information about the optical properties as well as, most notably, the geometric structure of the surface viewed. Knowledge of this structure, even if very approximate, will be of great help in land cover classification and in preparing surface roughness maps. For example, land cover classification techniques typically have problems distinguishing sparse forestlands with undergrowth from dense shrub land due to the similar biomass of the two cover types. The BRDF shape, however, is rather different for the two. An analysis should be able to pick up the prominent shadows cast by sparse trees (which determine the BRDF), allowing to distinguish them from the dense brush. See *Pinty and Verstraete* [1991] for a discussion of problems that may be associated with inversion of BRDF models.

Last but not least, changes in BRDF, albedo, or derived surface parameters can indicate change that may or may not be visible spectrally or spatially, thus adding to the information base from which to derive change maps for global change studies.

2.2. Operational Aspects of BRDF Modeling

When considering which type of BRDF model to employ for extensive BRDF and albedo analysis from observed data, a decision has to be made between physical, semiempirical, and empirical models. These differ in the detail with which they describe the physical processes responsible for light scattering in the scene, the degree of a priori knowledge one must have of the type of land cover encountered, and the number of observations needed to derive model parameters that describe the BRDF well in both viewing and illumination hemispheres. While physical models describe the scattering of light explicitly, empirical models do not attempt to explain it but rather describe the BRDF by any empirically suitable mathematical function. Naturally, physical BRDF models are considerably more complex than their empirical counterparts. In terms of complexity, semiempirical models are in between these two. As approximations to physical models they are mathematically much simpler, but they retain the more important of their characteristics. See *Strahler* [1994] for an overview of BRDF models.

In choosing between these model types, three things need to be considered, especially in the context of the operational needs of large-scale (e.g., global) BRDF and albedo processing. First, the information that has to go into the models is different. Empirical models, due to their nature, require many more observations than physical models over both viewing and illumination hemispheres if the BRDF shape is to be well fitted. In practice, however, the number of observations available from a space-based sensor in any given time period is constrained by orbital and instrument characteristics of the sensor and by cloud cover. Furthermore, BRDF may change over time and with season, so the period over which observations may be accumulated cannot be arbitrarily long.

Physical BRDF models avoid this problem. But, on the other hand, no physical model is equally suitable for every land cover type. For example, radiative transfer models are mostly better suited for horizontally homogeneous layers of

vegetation, and geometric-optical models, for discrete-crown canopies. As a consequence, applying physical models to global BRDF retrieval requires some external knowledge of the land cover types encountered so that the most suitable model can be selected for the analysis of each pixel.

The semiempirical BRDF models discussed in this paper represent a compromise here. While requiring more observations than physical models to accurately describe an observed BRDF, they require fewer than empirical models. The approximate physical basis on which they rest constrains in a meaningful way the possible BRDF shapes in unobserved regions of the viewing and illumination hemispheres. On the other hand, due to their potentially containing both volume-scattering and surface-scattering kernels, no pre-selection of models is necessary. In fact, given that they are not overly costly to compute, several semiempirical models can be processed in parallel to find the best fit.

Second, the type of model to be chosen may be dictated by the computing time required for data processing. If only a limited land area is to be investigated, using a complex physical model may well be feasible. But if a global data set is to be analyzed at a spatial resolution in the range of 1 km, as is planned for some of the EOS instruments (e.g., MODIS and MISR), physical models are presently very likely to be too costly by a large margin. Besides their intrinsic complexity, their inversion, if possible, requires numerical procedures that involve a large number of forward calls to the model per pixel, which greatly increases the computing cost. Given that there are 149 million km² of land surface on the Earth, 246 1-km pixels need to be processed each second in order to arrive at a global product after 7 full days. Assuming only 15 forward calls per inversion and a few bands to be processed, that would already imply some 15,000 BRDF model calls that need to be processed per second if a global land data set is to be processed in a week. Even fast computers are currently too slow to meet this demand, prohibiting at least for the time being the use of physical models for global kilometer-scale operational BRDF modeling. Linear semiempirical models, on the other hand, can be inverted analytically and albedo can be calculated from look-up tables (as discussed later in this paper) in only a fraction of the time needed for physical models.

A third constraint is given by the invertibility of the models. Inversion of physical models, generally not possible analytically, is more often than not made difficult due to problems inherent to numerical inversion schemes and may in some cases even be impossible. Furthermore, numerical inversion algorithms usually require initial estimates of the parameters to be deduced, and the results in some circumstances can depend on those estimates, making necessary further analysis. The optimal inversion scheme also depends on the specific model function used and the range of parameters encountered. Nonlinear semiempirical models are more stable in this respect but still easily show these problems. Due to their nature, however, linear kernel-driven models can be inverted analytically in a fast and efficient way, as discussed by P. Lewis (On the utility of linear, kernel-based BRDF models, manuscript in preparation; see also Lewis [1995]).

One can thus conclude that semiempirical models have several operational advantages over physical and purely em-

pirical models: (1) They are much faster to compute than full physical models; (2) they require only a limited number of observations to be invertible; and (3) if linear they may even be inverted analytically so that numerical problems are avoided altogether. But still these models encompass more meaning, and often fit observations better (as will be shown in a forthcoming paper by the authors) than purely empirical models. The parameters obtained from them have no direct meaning in terms of individual biophysical or structural parameters, but do characterize the prevailing type of scattering and give a general indication of the structural properties of the scene viewed.

Linear kernel-driven models, besides being operationally and computationally feasible, and efficiently invertible, also have the advantage of scaling spatially and being able to account easily for inhomogeneity in land cover at the subpixel scale. Whereas physical models usually assume homogeneous pixels, linear semiempirical models accommodate to some extent mixed BRDF signals due to the fact that they are superpositions of basic BRDF shapes if adjacency effects and multiple scattering between components are negligible. In global processing, especially at resolutions of a few kilometers, these are important additional advantages of linear semiempirical models.

As a consequence, both the European POLDER and the American MODIS/MISR BRDF and albedo products will rely most likely on linear kernel-driven models for deriving BRDF and albedo from the respective observations. Linear semiempirical models are, for the time being, the models of choice for operational BRDF processing on a global scale. In a demonstration of the capability of these models, *Leroy and Roujean* [1994] have successfully applied their model of this type to AVHRR data and have corrected it for sun and view angle effects.

In the remainder of this paper, three new kernels that are under consideration for these applications are introduced and discussed along previously published mathematical expressions for kernels.

3. Volume-Scattering Kernels (Radiative Transfer-Based)

3.1. Derivation of the Ross-Thick Kernel

The Ross-thick kernel has been derived and described by *Roujean et al.* [1992]. It is based on an approximation for large values of the leaf area index (LAI); a new approximation for small LAI will be given in the next section. Since this new approximation is based on the same formulas used by Roujean and coworkers, an outline of the respective calculations is provided here first.

In their derivation of this kernel, *Roujean et al.* [1992] start out from a formula taken from *Ross* [1981]. It gives the bidirectional reflectance above a horizontally homogeneous plant canopy calculated from radiative transfer theory in a single scattering approximation, meaning that no photon is scattered more than once on either leaves or the surface. The scattering facets, or leaves, are located randomly above a flat horizontal surface of Lambertian reflectance ρ_0 . Their volume density is N , their area σ , their Lambertian reflectance s , and their Lambertian transmittance t . The LAI of the canopy

is $LAI = N\sigma z_{\max}$, where z_{\max} is the maximal height of the canopy. If w is the volume scattering coefficient, $G(\theta)$ is the facets area orientation function for a ray incident with zenith θ and azimuth ϕ , and $P(\theta_i, \theta_v, \phi)$ is the phase function of the medium (i stands for illumination, v for view), the BRDF R_{vol} is given by

$$R_{vol} = \frac{w}{4N\sigma} \frac{P(\theta_i, \theta_v, \phi)}{\cos \theta_i \cos \theta_v} \cdot \frac{1 - \exp \left\{ -LAI \left[\frac{G(\theta_i)}{\cos \theta_i} + \frac{G(\theta_v)}{\cos \theta_v} \right] \right\}}{\frac{G(\theta_i)}{\cos \theta_i} + \frac{G(\theta_v)}{\cos \theta_v}} + \rho_0 \exp \left\{ -LAI \left[\frac{G(\theta_i)}{\cos \theta_i} + \frac{G(\theta_v)}{\cos \theta_v} \right] \right\}. \quad (1)$$

Assuming an isotropic distribution of facet orientations, we have $G(\theta_i) = G(\theta_v) = 1/2$, $w = N\sigma(s+t)/2$, and

$$P(\theta_i, \theta_v, \phi) = \frac{8}{3\pi} \frac{[(\pi - \xi) \cos \xi + \sin \xi] s + (-\xi \cos \xi + \sin \xi) t}{s + t}, \quad (2)$$

where ξ is the phase angle of scattering, and

$$\cos \xi = \cos \theta_i \cos \theta_v + \sin \theta_i \sin \theta_v \cos \phi. \quad (3)$$

Entering these relationships into (1) and furthermore assuming $s = t$ (leaf reflectance equals leaf transmittance), one arrives at

$$R_{vol} = \frac{4s}{3\pi} \frac{(\pi/2 - \xi) \cos \xi + \sin \xi}{\cos \theta_i + \cos \theta_v} \cdot \left(1 - \exp \left\{ -\frac{LAI}{2} (\sec \theta_i + \sec \theta_v) \right\} \right) + \rho_0 \exp \left\{ -\frac{LAI}{2} (\sec \theta_i + \sec \theta_v) \right\}. \quad (4)$$

At this point we make the approximation of an optically thick canopy, that is, $LAI \gg 1$. Then the value of LAI dominates the exponential function, and the variable zenith angles play only a minor role. The expression $1/2 (\sec \theta_i + \sec \theta_v)$ can be replaced by an average of this expression over the range of occurring angles. For $\theta_i = 0^\circ$, this expression is 1.0 for $\theta_v = 0^\circ$, 1.08 for $\theta_v = 30^\circ$, and 1.5 for $\theta_v = 60^\circ$; for $\theta_i = 30^\circ$ it is 1.15 for $\theta_v = 30^\circ$ and 1.58 for $\theta_v = 60^\circ$; for $\theta_i = 60^\circ$ it is 2.0 for $\theta_v = 60^\circ$. Thus, a typical value for the average $B = \langle 1/2 (\sec \theta_i + \sec \theta_v) \rangle$ is 1.5. Consequently, the BRDF expression for the thick approximation is

$$R_{thick} = \frac{4s}{3\pi} \frac{(\pi/2 - \xi) \cos \xi + \sin \xi}{\cos \theta_i + \cos \theta_v} \cdot (1 - \exp \{-LAI B\}) + \rho_0 \exp \{-LAI B\}. \quad (5)$$

It is the aim to create a kernel of the form $R = c_1 k_{thick} + c_2$, where k_{thick} is the Ross-thick kernel and c_1, c_2 are constants. Furthermore, it is desirable for the kernel to have the property $k_{thick}(\theta_i = 0^\circ, \theta_v = 0^\circ) = 0$, a convention introduced by Roujean *et al.* [1992]. Since the term containing all the geometric expressions is $\pi/4$ for nadir illumination and

viewing, the kernel will be defined as the geometric term less $\pi/4$. Then

$$R_{thick} = c_1 k_{thick} + c_2, \quad (6)$$

where the kernel is

$$k_{thick} = \frac{(\pi/2 - \xi) \cos \xi + \sin \xi}{\cos \theta_i + \cos \theta_v} - \frac{\pi}{4} \quad (7)$$

and the constants are

$$c_1 = \frac{4s}{3\pi} (1 - \exp \{-LAI B\}), \quad (8)$$

$$c_2 = \frac{s}{3} + \exp \{-LAI B\} \left(\rho_0 - \frac{s}{3} \right). \quad (9)$$

The constant c_1 will be the weight of the thick volume-scattering kernel in a complete kernel-driven model. The constant c_2 will be included in the isotropic scattering constant.

3.2. Derivation of the Ross-Thin Kernel

The derivation of the Ross-thin kernel starts out similar to the one of the Ross-thick kernel, but is done for small LAI. We start from (4).

The first term containing the exponential function refers to light scattered by the isotropically distributed and oriented leaves, modulated by the phase function of the canopy, and its attenuation traveling in and out. We approximate this expression for small values of LAI ($LAI \ll 1$) by exploiting $\exp\{x\} \approx 1 + x$. The second exponential function refers to the photons scattered by the layer beneath the canopy, for example, by the soil or other, much denser vegetation. Since we are aiming at an approximation for a thin canopy, we here assume that these photons are either absorbed or suffer multiple scattering and thus becomes isotropic. The second term of (4) is consequently replaced by the average Lambertian reflectance of the layer beneath the governing, thin canopy on top, ρ_l .

Then we arrive at

$$R_{thin} = \frac{4s}{3\pi} \frac{(\pi/2 - \xi) \cos \xi + \sin \xi}{\cos \theta_i + \cos \theta_v} \cdot \frac{LAI}{2} (\sec \theta_i + \sec \theta_v) + \rho_l. \quad (10)$$

Taking care of the cos and sec terms leads to

$$R_{thin} = \frac{2sLAI}{3\pi} \frac{(\pi/2 - \xi) \cos \xi + \sin \xi}{\cos \theta_i \cos \theta_v} + \rho_l. \quad (11)$$

Again, this kernel should be zero for nadir illumination and viewing, but the angle term in the above equation is $\pi/2$, so the kernel is the angle term less that number if it is to be normalized to zero for nadir illumination and viewing. This gives

$$R_{thin} = c_1 k_{thin} + c_2, \quad (12)$$

where the kernel is

$$k_{thin} = \frac{(\pi/2 - \xi) \cos \xi + \sin \xi}{\cos \theta_i \cos \theta_v} - \frac{\pi}{2} \quad (13)$$

and the constants are

$$c_1 = \frac{2sLAI}{3\pi} \quad (14)$$

$$c_2 = \frac{sLAI}{3} + \rho_l. \quad (15)$$

The constant c_1 will be the weight of the thin volume-scattering kernel in a complete kernel-driven model, and the constant c_2 will be included in the isotropic scattering constant.

Note that this kernel will also be applicable for cases with extremely high LAI, where the dense leaves of the canopy will act much like a solid surface, and scattering will mainly be dominated by the few leaves that protrude sparsely out of the top of the canopy.

4. Surface-Scattering Kernels (Geometric Optics-Based)

4.1. The Roujean Kernel

The derivation of the Roujean geometric-optical kernel is given by *Roujean et al.* [1992, appendix]. For completeness and reference, a brief summary suffices here.

The reflectance is modeled for a random arrangement of rectangular protrusions on a flat horizontal surface. The length of the protrusions is l , their height is h and their width b . All sunlit areas, ground and protrusions, are assumed to be equally bright with a reflectance ρ_0 . All shadows, both on the ground and on the protrusions, are perfectly black. Mutual shadowing is not taken into account; this restricts the zenith angles to a range from nadir to about 60° (this condition is derived by allowing the shadow cast to never be "outside" the base area of the protrusions, i.e., $lh \tan \theta_{i,v} \leq lb$). Furthermore, the side of the protrusions, of area bh , is neglected, which means the condition $l \gg h, l \gg b$ is imposed.

Then the reflectance is

$$R_{prot} = c_1 k_{prot} + c_2, \quad (16)$$

where the kernel is

$$k_{prot} = \frac{1}{2\pi} [(\pi - \phi) \cos \phi + \sin \phi] \tan \theta_i \tan \theta_v - \frac{1}{\pi} \left(\tan \theta_i + \tan \theta_v + \sqrt{\tan^2 \theta_i + \tan^2 \theta_v - 2 \tan \theta_i \tan \theta_v \cos \phi} \right). \quad (17)$$

This kernel is zero for nadir viewing and illumination. The constants are:

$$c_1 = \rho_0 \frac{h}{b}, \quad (18)$$

$$c_2 = \rho_0. \quad (19)$$

The constant c_1 will be the weight of the Roujean kernel in a complete kernel-driven model, the constant c_2 will be included in the isotropic scattering constant.

4.2. Derivation of the Li-Sparse Kernel

The basis of this kernel is the modeling approach developed by *Li and Strahler* [1986], where the reflectance of a scene is given by the areal proportions K of sunlit crown (reflectance C), sunlit ground (reflectance G), shaded crown (reflectance T), and shaded ground (reflectance Z). Note that the reflectances are reflectances as seen by the sensor at the given illumination condition, that is, these quantities may depend on the illumination angles themselves. So

$$R_{geo} = K_C C + K_G G + K_T T + K_Z Z. \quad (20)$$

However, in deducing this kernel it is assumed that the shadows are perfectly black, that is, $T = Z = 0$. Furthermore, it is assumed that sunlit ground and crown are equally bright, $C = G$. Then

$$R_{geo} = C (K_C + K_G), \quad (21)$$

and what remains to be done is to determine geometric expressions for the areas of sunlit crown, K_C , and sunlit ground, K_G .

The expression for sunlit ground, K_G , is easily derived. Boolean logic says that if one has objects of average area A , here the projection of the crowns onto the ground, so $A_{i,v} = A(\theta_i, \theta_v)$, and if these objects are randomly placed, the proportion of an area that is not covered by objects is $\exp(-\lambda A_{i,v})$, where $\lambda = n/A$ is the number density of objects, with n the number of objects [*Strahler and Jupp*, 1990]. The area of the objects overlapping randomly in the case of discrete crowns is the sum of the shadow of illumination and the shadow of viewing, minus the area O by which these two overlap:

$$K_G = \exp \{ -\lambda [A_i(\theta_i, \phi_i) + A_v(\theta_v, \phi_v) - O(\theta_i, \theta_v, \phi_i - \phi_v)] \}. \quad (22)$$

The areas $A_{i,v}$ of the illumination and viewing shadows can be easily determined individually if the crowns are assumed to be spheroids with vertical length $2b$, horizontal width $2r$, and distance h to their centers above the ground. First, a vertical-scale transformation is performed to make them spheres. This transformation replaces all zenith angles by "equivalent" zenith angles (primed: θ'), at which a sphere of radius r would have to be illuminated to produce the same shadow as the spheroid does when illuminated at the actual zenith angle. This transformation is $\theta' = \tan^{-1}(b/r \tan \theta)$. Then the length on the ground in illumination or viewing direction of the shadow of the sphere is $l = r/\cos \theta' = r \sec \theta'$, and the area of the shadow is $A = \pi r l = r^2 \sec \theta'$. So we have

$$K_G = \exp \{ -\lambda \pi r^2 [\sec \theta'_i + \sec \theta'_v - O(\theta_i, \theta_v, \phi_i - \phi_v)] \}. \quad (23)$$

The quantity O is all that needs to be determined to calculate K_G .

Consider first the case of the principal plane, that is, $\phi = 0$ or $\phi = \pi$. Then the elliptic viewing and illumination

projections of the crown on the ground overlap along their major axis (if they overlap). The area of the segment cut off from each ellipse by the line connecting the two intersection points, which is perpendicular to the major axis, is given by

$$F = cd \cos^{-1}(x/c) - xy, \quad (24)$$

where c and d are the major and minor axis lengths, and x and y are the Cartesian coordinates of one of the intersection points. In our case, $c = r \sec \theta'$ and $d = r$. The variables x and y are expressed indirectly by a parameter t by parametrizing the ellipses as $x = c \cos t$, $y = d \sin t$ (so $(x/c)^2 + (y/d)^2 = 1$, as should be). The area cut off from each ellipse then is $F = r^2 \sec \theta' \cos^{-1}(\cos t) - r^2 \sec \theta' \cos t \sin t$. The overlap area sought is the sum of the two cutoff segments,

$$O = F_i + F_v = r^2 (\sec \theta_i + \sec \theta_v) (t - \cos t \sin t). \quad (25)$$

In this way, K_G now is expressed in a way that depends only on the parameter t . Note that the values of t for the intersection points of the two ellipses may be set equal since they refer to the circle from which the ellipses can be seen to have been expanded in the parametrization.

The parameter t is still needed; it is found from the actual distance $h'D$ between the two centers of the ellipses, once expressed by geometric proportions, once by the parameter t ; h' is the rescaled height of the sphere, $h' = hr/b$. The first version is given by $h'D = |h' \tan \theta'_i - h' \tan \theta'_v \cos \phi|$, since $h' \tan \theta'$ is the distance from the stem to the center of the respective ellipse. The term $\cos \phi$ takes care of cases where the shadow centers are on opposite sides of the stem and one needs to add the lengths instead of subtracting them. The second way of expressing the length $h'D$ is as the sum of the two distances along the axes of overlap up to the line connecting the points of intersection, expressed by the parameter t : $h'D = x_i + x_v = a_i \cos t + a_v \cos t = r \sec \theta'_i \cos t + r \sec \theta'_v \cos t = r(\sec \theta'_i + \sec \theta'_v) \cos t$. Now these two expressions for $h'D$ are equated, and the equation is solved for $\cos t$, resulting in

$$\cos t = \frac{h}{b} \frac{|\tan \theta'_i - \tan \theta'_v \cos \phi|}{\sec \theta'_i + \sec \theta'_v}. \quad (26)$$

Using this equation together with the one for O , equation (25), gives the exact overlap on the principal plane.

Now let us look at the situation for arbitrary values of ϕ . The approximation made for this case is that (24) still holds even though the areas cut off of the ellipses by the overlap no longer are aligned with one of the principal axes. The distance $h'D$ between the centers of the ellipses is now given by $D = (\tan^2 \theta'_i + \tan^2 \theta'_v - 2 \tan \theta'_i \tan \theta'_v \cos \phi)^{1/2}$, and the sum of the two axes of the ellipses taken along D is $r(\sec \theta'_i + \sec \theta'_v) / (1 + u^2)^{1/2}$, where $h'u = h' \tan \theta_i \tan \theta_v \sin \phi / D$ may be interpreted as the distance of the line D from the base of the tree. Proceeding with the approximation, we obtain $h'D = r(\sec \theta'_i + \sec \theta'_v) \cos t / (1 + u^2)^{1/2}$, or

$$\cos t = \frac{h}{b} \frac{\sqrt{D^2 + (\tan \theta'_i \tan \theta'_v \sin \phi)^2}}{\sec \theta'_i + \sec \theta'_v}, \quad (27)$$

in which D is known. Note that this equation reduces to (26)

for $\phi = 0$ or $\phi = \pi$, since then $\sin \phi = 0$ and $\cos \phi = \pm 1$, so that $\tan^2 \theta'_v = (\tan \theta'_v \cos \phi)^2$, reducing D from above to the formula for D on the principal plane. It also converges to the exact solution on the principal cone ($\theta_i = \theta_v$) for small values of D .

With K_G known, the fraction of sunlit crown area, K_C , remains to be determined. Here the problem encountered is that due to mutual shadowing, shadows from adjacent crowns fall onto any given crown onto areas that otherwise would be sunlit. Since we wish to derive an approximation for a sparse canopy, we may neglect this effect. It does not play a major role in the case under consideration. Then determining K_C is not difficult, as can be seen from the following.

The area of a crown that is both illuminated and viewed can be calculated as follows. The area seen (of the spheroid rescaled to be a sphere) is $F_v = \pi r^2 \sec \theta'_v$. How much of it is sunlit depends on the phase angle ξ' between illumination and viewing direction, given by $\xi' = \cos \theta'_i \cos \theta'_v + \sin \theta'_i \sin \theta'_v \cos \phi$. The area diminishes as $\cos^2(\xi'/2) = (1 + \cos \xi)/2$, where the \cos^2 stems from the fact that the sphere is rounded in two spatial directions, and the argument is $\xi'/2$, since everything will be illuminated if view and illumination angles coincide, and nothing will be illuminated, not at $\xi' = 90^\circ$, but at $\xi' = 180^\circ$. Thus the illuminated and viewed area of a single crown is $F_C = \pi r^2 \sec \theta'_v (1 + \cos \xi)/2$. The sunlit and viewed crown area of n trees will, however, not be nF_C , since random overlapping of the sunlit and viewed areas of the individual crowns will occur. Using Boolean logic [Strahler and Jupp, 1990], where $\exp(-\lambda A_v)$ is the probability of not seeing crown areas, that is, $(1 - \exp(-\lambda A_v))$ is the probability of seeing crown area, we have

$$K_C = (1 - \exp\{-\lambda \pi r^2 \sec \theta'_v\}) \frac{1}{2} (1 + \cos \xi'). \quad (28)$$

Now the expression for the reflection in the sparse approximation can be given in full:

$$\begin{aligned} R_{sparse} &= C(K_C + K_G) \\ &= C \left((1 - \exp\{-\lambda \pi r^2 \sec \theta'_v\}) \frac{1}{2} (1 + \cos \xi') \right. \\ &\quad \left. + \exp\{-\lambda \pi r^2 [\sec \theta'_i + \sec \theta'_v - O(\theta_i, \theta_v, \phi)]\} \right). \end{aligned} \quad (29)$$

Since λ is a small number in the sparse approximation, we can approximate $\exp\{x\} \approx 1 + x$ and arrive at

$$\begin{aligned} R_{sparse} &= C \left(\lambda \pi r^2 \sec \theta'_v \frac{1}{2} (1 + \cos \xi') + 1 \right. \\ &\quad \left. - \lambda \pi r^2 [\sec \theta'_i + \sec \theta'_v - O(\theta_i, \theta_v, \phi)] \right), \end{aligned} \quad (30)$$

and finally, since the angle term already vanishes for nadir viewing and illumination,

$$R_{sparse} = c_1 k_{sparse} + c_2, \quad (31)$$

where

$$k_{sparse} = O(\theta_i, \theta_v, \phi) - \sec \theta'_i - \sec \theta'_v + \frac{1}{2} (1 + \cos \xi') \sec \theta'_v, \quad (32)$$

and

$$O = \frac{1}{\pi} (t - \sin t \cos t) (\sec \theta'_i + \sec \theta'_v), \quad (33)$$

$$\cos t = \frac{h \sqrt{D^2 + (\tan \theta'_i \tan \theta'_v \sin \phi)^2}}{b \sec \theta'_i + \sec \theta'_v}, \quad (34)$$

$$D = \sqrt{\tan^2 \theta'_i + \tan^2 \theta'_v - 2 \tan \theta'_i \tan \theta'_v \cos \phi}, \quad (35)$$

$$\cos \xi' = \cos \theta'_i \cos \theta'_v + \sin \theta'_i \sin \theta'_v \cos \phi, \quad (36)$$

$$\theta' = \tan^{-1} \left(\frac{b}{r} \tan \theta \right), \quad (37)$$

and

$$c_1 = C \lambda \pi r^2, \quad (38)$$

$$c_2 = C. \quad (39)$$

The constant c_1 will be the weight of the sparse surface-scattering kernel in a complete kernel-driven model, and the constant c_2 will be included in the isotropic scattering constant.

This kernel is not linear yet in that it still contains two parameters, namely the ratios b/r and h/b describing crown shape and relative height. This kernel therefore actually represents a family of kernels, governed by the values of these two internal parameters. In linear applications these could be set to one or two fixed values each, for example, slightly oblate (or round) crowns and prolate crowns, and low or high crowns. This would give four distinctive kernels that may then be used in linear models. The difference between these kernels will be discussed in section 5.1.

4.3. Derivation of the Li-Dense Kernel

In contrast to the situation for the sparse canopy, mutual shadowing cannot be disregarded in the dense canopy case. *Li and Strahler* [1992] discuss two extreme cases of canopy structure with respect to mutual shadowing: the case of a canopy with uniform tree heights and the case of a canopy with random tree heights. The first case is not of interest here, since it is similar to a radiative transfer situation: a dense canopy of uniform height can be approximated by a plane-parallel horizontally layered canopy. So we choose to deduce this kernel for the case of random tree heights. *Li and Strahler* [1992] showed that in this case, including mutual shadowing, the ratio of the crown area viewed and sunlit and all area that is not illuminated background is the same for the canopy case as for a single crown ($f = F = K_C / (1 - K_G)$), where F refers to the case of a single crown and f to that of many crowns.

Again, the reflectance is modeled as in (20). Assuming perfectly black shadows, $T = Z = 0$, results in

$$R_{geo} = C K_C + G K_G. \quad (40)$$

Then, introducing F , we get

$$R_{dense} = C F (1 - K_G) + G K_G. \quad (41)$$

The quantity F can be easily deduced. The area of a viewed crown is $A_v = \pi r^2 \sec \theta'_v$, with notations as for the sparse kernel, and, as above only a portion $1/2(1 + \cos \xi')$ of this area will be sunlit. So the viewed and sunlit area of a single crown is $A_C = \pi r^2 \sec \theta'_v / 2(1 + \cos \xi')$. All area not sunlit ground is given by the sum of the areas of viewing and illumination shadow, minus their overlap. As discussed for the sparse kernel, this is, for a single crown, $1 - A_G = \pi r^2 (\sec \theta'_v + \sec \theta'_i - O(\theta'_i, \theta'_v))$, where O is the area of overlap. Thus we have

$$f = F = \frac{1/2(1 + \cos \xi') \sec \theta'_v}{\sec \theta'_v + \sec \theta'_i - O(\theta'_i, \theta'_v)}. \quad (42)$$

Furthermore, the areal fraction K_G of sunlit ground for the whole canopy is, again, as before,

$$K_G = \exp \left\{ -\lambda \pi r^2 [\sec \theta'_i + \sec \theta'_v - O(\theta_i, \theta_v, \phi_i - \phi_v)] \right\}. \quad (43)$$

This exponential term is very small in a dense canopy, since λ is large; this simply means that almost no sunlit ground is visible, as is appropriate for a dense canopy. However, an additional argument may be added to disregarding the contribution of K_G . To see this, assume $C = G$, which can be done without large error since K_G is small anyway. Then

$$R_{dense} = C (F(1 - K_G) + K_G) = C (F + (1 - F) K_G). \quad (44)$$

Here, not only is K_G very small, but $1 - F$ is small, too, since F is a fraction of 1. So this product of two small quantities is negligible, and we arrive at

$$R_{dense} = C F = \frac{C}{2} \frac{(1 + \cos \xi') \sec \theta'_v}{\sec \theta'_v + \sec \theta'_i - O(\theta'_i, \theta'_v)}, \quad (45)$$

which is the same as if we had set $K_G = 0$ immediately, but secured by an additional argument for the validity of this approximation.

Thus the reflectance is

$$R_{dense} = c_1 k_{dense} + c_2, \quad (46)$$

where the kernel is

$$k_{dense} = \frac{(1 + \cos \xi') \sec \theta'_v}{\sec \theta'_v + \sec \theta'_i - O(\theta'_i, \theta'_v)} - 2, \quad (47)$$

making it zero for nadir viewing and illumination, and where as above for the sparse kernel,

$$O = \frac{1}{\pi} (t - \sin t \cos t) (\sec \theta'_i + \sec \theta'_v), \quad (48)$$

$$\cos t = \frac{h \sqrt{D^2 + (\tan \theta'_i \tan \theta'_v \sin \phi)^2}}{b \sec \theta'_i + \sec \theta'_v}, \quad (49)$$

$$D = \sqrt{\tan^2 \theta'_i + \tan^2 \theta'_v - 2 \tan \theta'_i \tan \theta'_v \cos \phi}, \quad (50)$$

$$\cos \xi' = \cos \theta'_i \cos \theta'_v + \sin \theta'_i \sin \theta'_v \cos \phi, \quad (51)$$

$$\theta' = \tan^{-1} \left(\frac{b}{r} \tan \theta \right), \quad (52)$$

and the constants are

$$c_1 = \frac{C}{2}, \quad (53)$$

$$c_2 = C. \quad (54)$$

One other possibility would be not to set $K_G = 0$, but to give it a more realistic constant value χ . Then the constants would be

$$c_1 = \frac{C}{2} (1 - \chi), \quad (55)$$

$$c_2 = C + (G - C)\chi. \quad (56)$$

Again the constant c_1 will be the weight of the dense surface scattering kernel in a complete kernel-driven model, and the constant c_2 will be included in the isotropic scattering constant.

Similar to the sparse kernel, this dense kernel still contains two parameters, the ratios b/r and h/b describing crown shape and relative height, for which one may later choose two fixed values.

5. Kernel-Driven Models

5.1. The Kernels in Comparison

Before forming linear combinations of the kernels derived to create BRDF models, it is important to compare their shapes to see whether they are sufficiently different from one another to warrant using them in linear superpositions. Figures 1 and 2 show the shape of the kernels along and perpendicular to the principal plane; the kernel values were computed for $b/r = 1$ and $h/b = 2$. While the radiative transfer-based kernels are shaped like an upturned bowl, the geometric-optical kernels have the shape of downturned bowls. This difference occurs because the geometric-optical kernels are driven by the way shadows emerge and are hidden in a discrete-crown canopy, leading to a drop-off of the reflectance as viewing moves away from the direction of illumination. The radiative transfer-based kernels, on the other hand, are governed by the phase function and distribution of facet orientations of scattering centers, leading to an increase in reflectance with zenith angle. The two Ross approximations are somewhat similar close to nadir, but the Ross-thin approximation provides for a much faster rise of the reflectance for off-nadir zenith angles. The Li kernels show a considerably more pronounced hotspot than the Roujean kernel and have a more complex shape. Most notably, they avoid the unphysical behavior of the Roujean kernel at large zenith angles by taking into account mutual shadowing. Remotely sensed data obtained, for example, at high geographical latitudes can encompass this angular range, and the shape of kernels at large zenith angles is also important when calculating albedo from a model fitted to data. With respect to the difference between the Li-sparse and the Li-dense approximations, it is obvious from both the principal plane and cross principal plane plots that they are not linearly dependent.

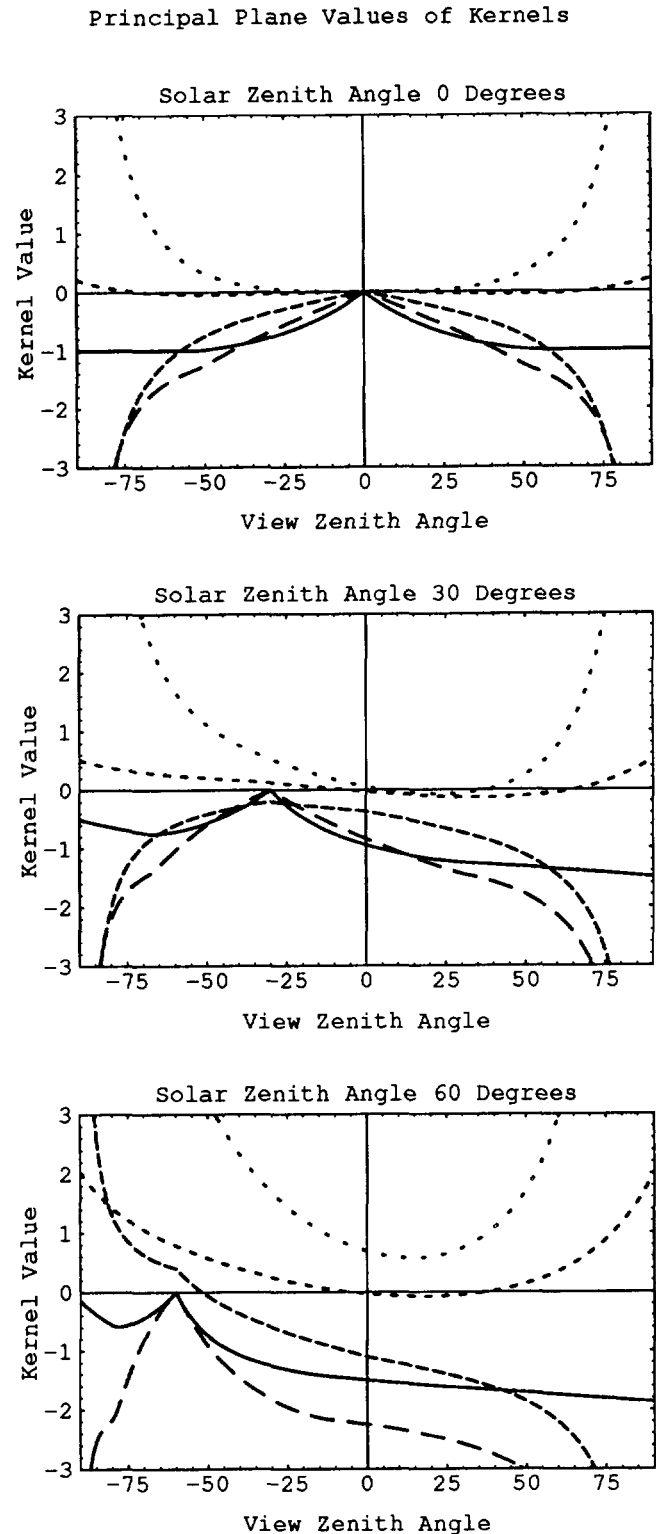


Figure 1. Principal plane values of the kernels for three different solar zenith angles. Lines of increasing dash length represent the Ross-thin, Ross-thick, Roujean, Li-sparse, and Li-dense kernel. The Li kernels are calculated for $b/r = 1$ and $h/b = 2$.

Figures 3 and 4 demonstrate the dependence of the Li kernels on the two internal parameters they contain, where it is suggested that for linear modeling these may be set to, for example, two different values each, producing four variants

Cross Principal Plane Values of Kernels

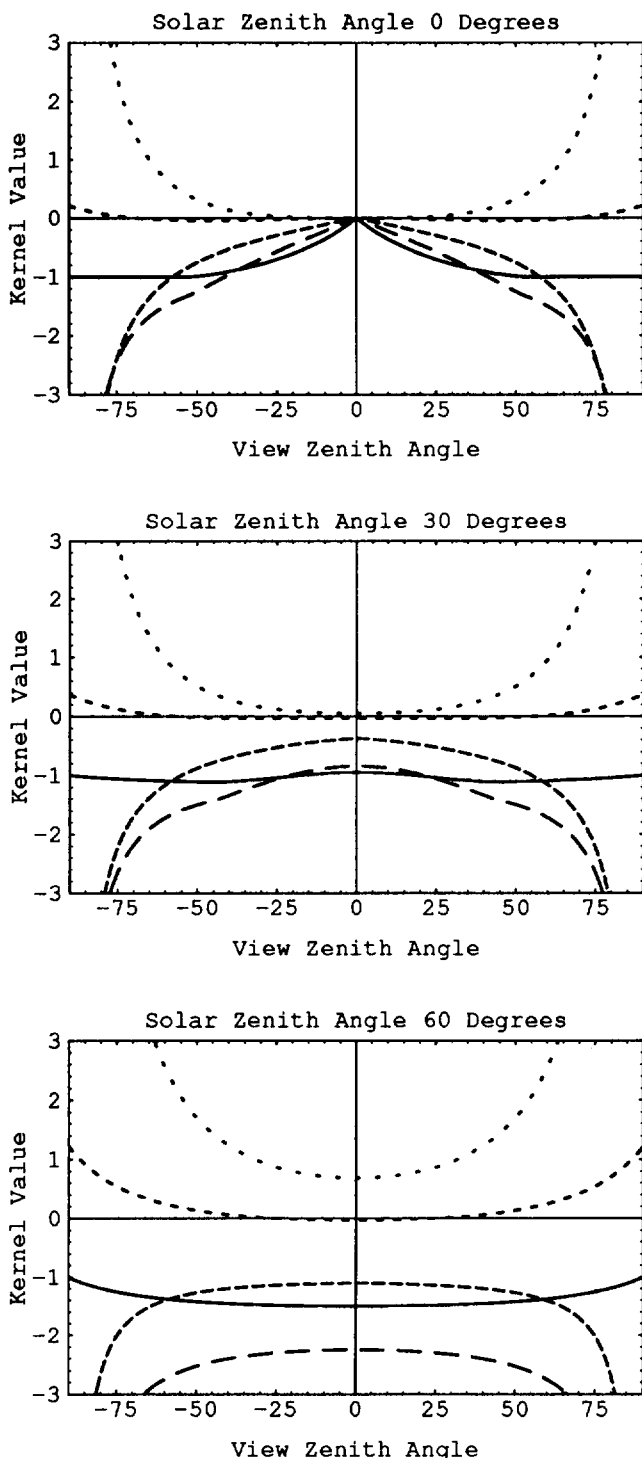


Figure 2. Cross principal plane values of the kernels for three different solar zenith angles. Lines of increasing dash length represent the Ross-thin, Ross-thick, Roujean, Li-sparse, and Li-dense kernel. The Li kernels are calculated for $b/r = 1$ and $h/b = 2$.

of each kernel. The values chosen here are $b/r = 0.75$ and $b/r = 2.5$ for crown shape, representing a slightly oblate, still rather round crown, and a prolate crown; the values chosen for relative height are $h/b = 1.5$ and $h/b = 2.5$,

Principal Plane Values of Li-Kernels for Different Values of Crown Shape and Height

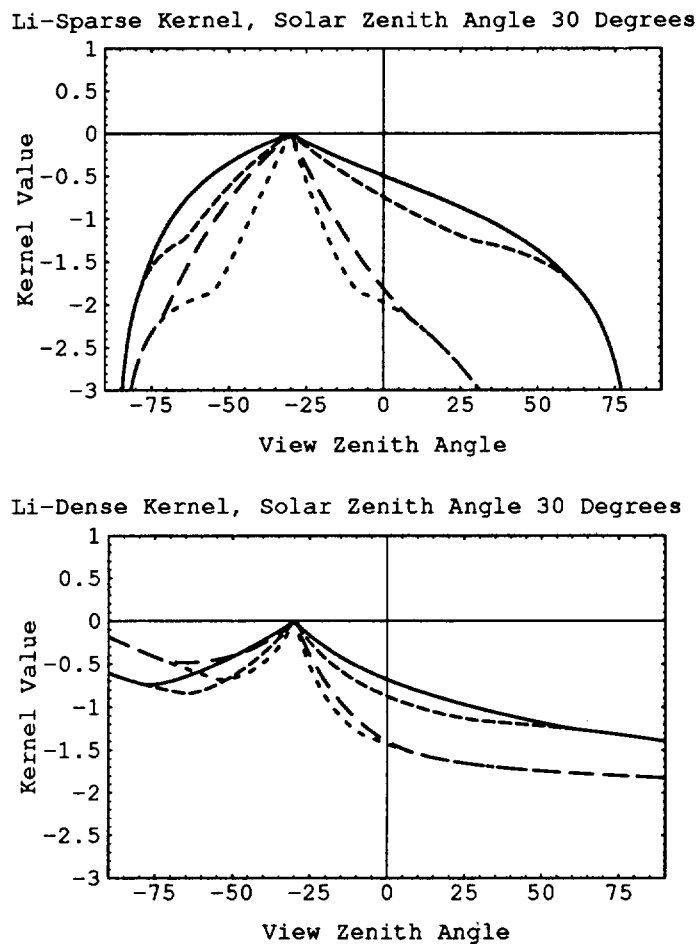


Figure 3. Variation of the Li-sparse and Li-dense kernels with parameters b/r and h/b along the principal plane. Lines of increasing dash length represent $b/r = 2.5, h/b = 2.5$ (tall prolate case); $b/r = 0.75, h/b = 2.5$ (tall slightly oblate case); $b/r = 2.5, h/b = 1.5$ (low prolate case); and $b/r = 0.75, h/b = 1.5$ (low slightly oblate case).

representing a low and a high case. For the Li-sparse kernel it is easily seen that the shapes of the kernel along the principal plane differ for the four parameter combinations, justifying their use as distinct kernels. For the cross principal plane there is not much difference, though, between kernels with different height parameters but the same crown shape. For the Li-dense kernel the differences are not as marked along the principal plane; however, looking at the cross principal plane it can be seen that there still is a qualitative difference involved with respect to crown shape. But overall, two variants of this kernel, representing the two different b/r ratios, should suffice.

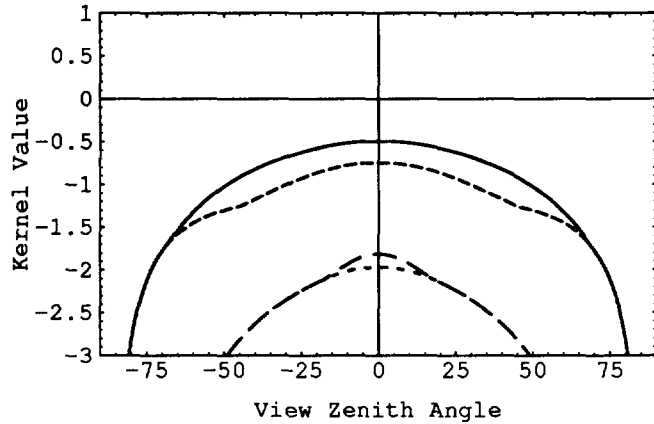
5.2. Synopsis of Semiempirical Model Factors

A complete linear semiempirical model is formulated as a linear combination of kernels. Most suitably it has the form

$$R = f_{iso} + f_{geo} k_{geo} + f_{vol} k_{vol}, \tag{57}$$

Cross Principal Plane Values of Li-Kernels for Different Values of Crown Shape and Height

Li-Sparse Kernel, Solar Zenith Angle 30 Degrees Ross-thick plus Roujean:



Li-Dense Kernel, Solar Zenith Angle 30 Degrees

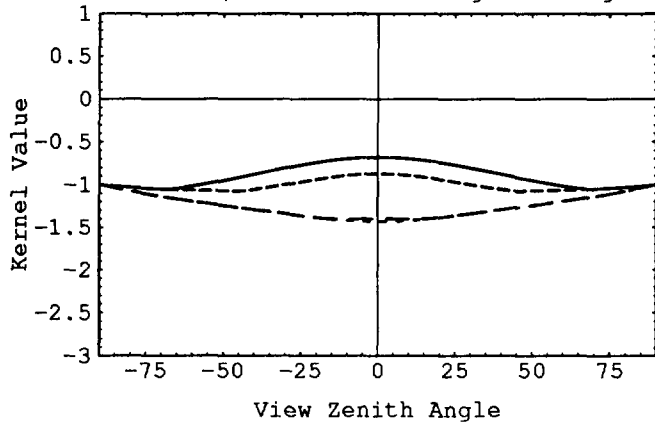


Figure 4. Variation of the Li-sparse and Li-dense kernels with parameters b/r and h/b along the cross-principal plane. Lines of increasing dash length represent $b/r = 2.5, h/b = 2.5$ (tall prolate case); $b/r = 0.75, h/b = 2.5$ (tall slightly oblate case); $b/r = 2.5, h/b = 1.5$ (low prolate case); and $b/r = 0.75, h/b = 1.5$ (low slightly oblate case).

which is derived from adding an appropriate choice of a geometric-optical and of a radiative transfer kernel, multiplied by the areal proportion of α or $(1 - \alpha)$ of land cover representing one or the other type of scattering (note that other interpretations of the parameter α are possible). The quantities k_{geo} and k_{vol} are the respective kernels. The factors f , which are the respective weights of the kernels (f_{iso} is the isotropic contribution), are then given by the following expressions, depending on the model.

Ross-thin plus Roujean:

$$f_{iso} = \alpha \rho_0 + (1 - \alpha) \left(\frac{sLAI}{3} + \rho_l \right), \quad (58)$$

$$f_{geo} = \alpha \rho_0 \frac{h}{b}, \quad (59)$$

$$f_{vol} = (1 - \alpha) \frac{2sLAI}{3\pi}. \quad (60)$$

$$f_{iso} = \alpha \rho_0 + (1 - \alpha) \cdot \left(\frac{s}{3} + \exp \{-LAI B\} \left(\rho_0 - \frac{s}{3} \right) \right), \quad (61)$$

$$f_{geo} = \alpha \rho_0 \frac{h}{b}, \quad (62)$$

$$f_{vol} = (1 - \alpha) \frac{4s}{3\pi} (1 - \exp \{-LAI B\}). \quad (63)$$

Ross-thin plus Li-sparse:

$$f_{iso} = \alpha C + (1 - \alpha) \left(\frac{sLAI}{3} + \rho_l \right), \quad (64)$$

$$f_{geo} = \alpha C \lambda \pi r^2, \quad (65)$$

$$f_{vol} = (1 - \alpha) \frac{2sLAI}{3\pi}. \quad (66)$$

Ross-thick plus Li-sparse:

$$f_{iso} = \alpha C + (1 - \alpha) \cdot \left(\frac{s}{3} + \exp \{-LAI B\} \left(\rho_0 - \frac{s}{3} \right) \right), \quad (67)$$

$$f_{geo} = \alpha C \lambda \pi r^2, \quad (68)$$

$$f_{vol} = (1 - \alpha) \frac{4s}{3\pi} (1 - \exp \{-LAI B\}). \quad (69)$$

Ross-thin plus Li-dense:

$$f_{iso} = \alpha C + (1 - \alpha) \left(\frac{sLAI}{3} + \rho_l \right), \quad (70)$$

$$f_{geo} = \alpha \frac{C}{2}, \quad (71)$$

$$f_{vol} = (1 - \alpha) \frac{2sLAI}{3\pi}. \quad (72)$$

Ross-thick plus Li-dense:

$$f_{iso} = \alpha C + (1 - \alpha) \cdot \left(\frac{s}{3} + \exp \{-LAI B\} \left(\rho_0 - \frac{s}{3} \right) \right), \quad (73)$$

$$f_{geo} = \alpha \frac{C}{2}, \quad (74)$$

$$f_{vol} = (1 - \alpha) \frac{4s}{3\pi} (1 - \exp \{-LAI B\}). \quad (75)$$

5.3. A Linear Empirical Model (The Modified Walthall Model)

Empirical models can be understood as being of the kernel-driven model type as well, where the kernels are empirical functions. An example is the modified Walthall model, derived by Walthall *et al.* [1985] and improved by Nilson and Kuusk [1989]. It has the form

$$R = p_0 (\theta_i^2 + \theta_v^2) + p_1 \theta_i^2 \theta_v^2 + p_2 \theta_i \theta_v \cos(\phi) + p_3. \quad (76)$$

Other modifications of this model might include, for example, terms employing the cosines of the zenith angles.

In the context of the current paper it is important that this model has the same form as the semiempirical models discussed above; it is comprised of a weighted superposition of functions of the angles, where the weights are the parameters of the model. As a consequence, models like the modified Walthall model can be processed along with linear semiempirical models by the same linear inversion scheme.

5.4. Advantages of Linearity

Some advantages of linear models in terms of global data processing have already been mentioned. Linearity in BRDF models has been comprehensively discussed by P. Lewis (On the utility of linear, kernel-based BRDF models, manuscript in preparation; see also *Lewis* [1995]) and demonstrated with the modified Walthall model.

First, any linear model can be inverted analytically through matrix inversion for the system of equations setting the derivative of the error function to zero. This provides direct estimates of the parameters f_{iso} , f_{geo} , and f_{vol} while avoiding numerical inversion problems.

Second, both the directional-hemispherical and bihemispherical integrals of the BRDF (“black sky” and “white sky” albedos, from which albedos for given conditions of direct illumination and diffuse skylight may be interpolated depending on the prevalent respective clearness or hazyness of the sky [see *Strahler et al.*, 1995]) may be precalculated for each kernel individually. The albedo of a model then is simply the weighted sum of the kernel albedos, where the weights are the same as were used in constructing the BRDF. By using a look-up table, numerical integration of the models can thus be avoided.

Third, linear BRDF models scale linearly in space if adjacency effects are assumed to be small. This allows for mixed pixel cases, as indicated by the areal proportion parameter α in the model factors listed in section 5.2. This feature also allows scaling BRDF and albedo from one spatial resolution up to a coarser one, for example, to a particular resolution needed for a climate model. In an alternate interpretation of the parameter α , linear models allow for land cover types that display both a volume scattering and a geometric optical contribution to the BRDF (neglecting multiple scattering between these two components).

Finally, since some of the parameters driving the models depend on wavelength while others do not (e.g., if they are structural), it may be possible to extract information on some of them from multiband analysis, making assumptions about the others. For instance, for the Ross-thin plus Li-dense model, the variation of f_{geo} directly reflects the variation of the sunlit component signature C with wavelength, since all other quantities entering do not depend on spectral band.

These advantages of formulating BRDFs as a weighted sum of fixed kernels need to be viewed in the light of the basic assumption underlying the approach, namely that BRDFs can be composed from such a superposition. A superposition may be justified for two reasons. First, a pixel that is made up at the subpixel level of, for example, a forest and a field of

wheat, should have a BRDF that reflects both surface and volume scattering, each of the two components stemming from the respective subpixel surface type. But equally important, even a scene composed of only one uniform cover type may display both types of scattering behavior. A forest canopy, for instance, will be dominated by geometric-optical surface scattering caused by the surfaces of the discrete crowns composing the forest. However, light entering the crowns will experience scattering inside the crowns that is more of a volume scattering type before exiting, adding this component to the signal. Indeed, a complex physical hybrid model combining surface and volume scattering in one model has been developed to describe this case [*Li et al.*, 1995].

What the superposition approach neglects to take into consideration is the interaction of the two components, surface and volume scattering: in the case of subpixel differences in the cover type, such interaction takes the form of adjacency effects, in the case of a volume and surface scattering uniform canopy it is due to the fact that the source of the light to one type of scattering is partly the radiation coming from the other type of scattering. While the adjacency effects are probably only minor in most cases except at very large zenith angles, the coupling of the two terms in the other situation is more problematic. However, even in this case the most simple first-order approach is superposition of two components assumed to be distinct. Ultimately, an important factor in judging this question is to demonstrate that the concept of kernel-driven models serves well in modeling BRDFs observed in the field, as is the case (as we will show in a forthcoming paper).

5.5. Nonlinear Semiempirical Models (The Rahman Model)

It is important to point out that semiempirical models need not necessarily be linear combinations of kernels, as is already indicated by the two kernel-internal parameters present in the Li kernels. Neither are semiempirical models necessarily derived from approximating more extensive physical theories.

An example for this is the semiempirical model introduced by *Rahman et al.* [1993], which we discuss here briefly because it demonstrates an alternate approach to semiempirical BRDF modeling that has interesting potential. Starting out from a two-parameter, purely empirical model by *Minnaert* [1941] for the reflectance of the surface of the moon, *Rahman et al.* improved the model by adding semiempirical elements that allow more realistic BRDF shapes. First, *Minnaert's* model is slightly altered to give a better basic BRDF shape; the BRDF is governed by the two parameters surface reflectance and k , governing the steepness of the BRDF dependence on the zenith angles. In a second step, a Henyey-Greenstein function is multiplied to the model to better represent forward and backward scattering. Finally, a hotspot term is multiplied to the expression which has a form inspired by the mathematical terms found in physical models with a hotspot. Both of these last additions also introduce a dependence of the BRDF on relative azimuth that was not present in the original model, thus making it considerably more realistic.

It is interesting how the Rahman model is built up from an empirical core, adding physically meaningful terms, while

the semiempirical models derived in this paper were derived by severely simplifying physical models. The model is an obvious alternative to linear models and, due to the way it was constructed, capable of adapting to a large variety of BRDF shapes. However, it is not of the kernel-driven type that is the focus of this paper. In applications it requires numerical inversion, which may be a major problem in global fine-scale applications.

6. Summary and Conclusions

As sensors capable of viewing the Earth's surface from various angles begin to play an important role in land remote sensing, analysis of the BRDF of each pixel is necessary for being able to compare observations obtained at different angles or standardizing observations to a common geometric situation. However, the BRDF found also contains otherwise untapped information. It allows precise deduction of the directional-hemispherical and bihemispherical integrals of the BRDF ("albedos") and inference of general surface properties, most notably coarse structural characteristics [e.g., *Li and Strahler*, 1986].

Operational considerations, such as computing resources, the problem of needing or not needing a priori land cover knowledge, invertibility and number of observations required, make linear semiempirical models prime candidates for large area BRDF analyses at a spatial resolution of the order of 1 km. Such kernel-driven models will, for example, be employed for BRDF evaluation and albedo deduction for the MODIS sensor of NASA's Earth Observing System (in combination with data from the MISR sensor on the same platform) [see *Strahler et al.*, 1995; *Wanner et al.*, 1995].

Kernel-driven models are based either on BRDF functions derived from approximations to physical BRDF models or on empirical functions. BRDFs are formulated through linear combinations of these functions, where ideally an isotropic constant is combined with a radiative transfer-based volume scattering kernel and a geometric optics-based surface scattering kernel. This paper briefly summarizes existing kernels, the large-LAI approximation to Ross' [1981] radiative transfer theory, *Roujean et al.*'s [1992] geometric optical model of rectangular protrusions, and the modified Walthall functions [*Walthall et al.*, 1985; *Nilson and Kuusk*, 1989]. It newly introduces three kernels that were previously given without deduction in a report by *Strahler et al.* [1994; updated 1995]. These are a low-LAI approximation to Ross' theory and two approximations to the *Li and Strahler* [1992] geometric optical mutual shadowing model for ensembles of distinct crowns, one for dense canopies and one for sparse canopies.

Together, these kernels allow formulating a number of semiempirical BRDF models suitable for global BRDF analysis. They also are important elements of upcoming land BRDF studies on the continental scale.

In a forthcoming paper the authors will demonstrate how these models perform on observed BRDF data sets and how land cover types differ in how well the individual models fit the data. All models will be shown to perform well in cases appropriate for them, thus validating them.

Code for scientific forward modeling and inversion of all of the models discussed in this paper may be obtained from the authors.

Acknowledgments. We thank M. Barnsley, P. Lewis and J.-P. Muller for hospitality during stimulating visits to University College London and for many discussions. Thanks to Baoxin Hu for diligent checking of code. This work was supported by NASA under NAS5-31369.

References

- Barnsley, M. J., A. H. Strahler, K. P. Morris, and J.-P. Muller, Sampling the surface bidirectional reflectance distribution function (BRDF), 1, Evaluation of current and future satellite sensors, *Remote Sens. Rev.*, **8**, 271–311, 1994.
- Cihlar, J., D. Manak, and N. Voisin, AVHRR bidirectional reflectance effects and compositing, *Remote Sens. Env.*, **48**, 77–88, 1994.
- Gerstl, S. A. W., and C. Simmer, Radiation physics and modeling for off-nadir satellite-sensing of non-Lambertian surfaces, *Remote Sens. Env.*, **20**, 1–29, 1986.
- Gutman, G., Normalization of multi-annual global AVHRR reflectance data over land surfaces to common sun-target-sensor geometry, *Adv. Space Res.*, **14**(1), 121–124, 1994.
- Leroy, M., and J.-L. Roujean, Sun and view angle corrections on reflectances derived from NOAA/AVHRR data, *IEEE Trans. Geosci. Remote Sens.*, **32**, 684–697, 1994.
- Lewis, P., The utility of kernel-driven BRDF models in global BRDF and albedo studies, *Proc. Int. Geosci. Remote Sens. Symp.*, **95**, 1186–1188, 1995.
- Li, X., and A. H. Strahler, Geometric-optical bidirectional reflectance modeling of a conifer forest canopy, *IEEE Trans. Geosci. Remote Sens.*, **24**, 906–919, 1986.
- Li, X., and A. H. Strahler, Geometric-optical bidirectional reflectance modeling of the discrete crown vegetation canopy: effect of crown shape and mutual shadowing, *IEEE Trans. Geosci. Remote Sens.*, **30**, 276–292, 1992.
- Li, X., A. H. Strahler, and C. E. Woodcock, A hybrid geometric optical-radiative transfer approach for modeling albedo and directional reflectance of discontinuous canopies, *IEEE Trans. Geosci. Remote Sens.*, **33**, 466–480, 1995.
- Li, Z., and A. Wu, Visible and near-IR bidirectional reflectance distribution over land from NOAA AVHRR, *Proc. 7th Conf. Sat. Met. Ocean*, 336–337, 1994.
- Minnaert, M., The reciprocity principle in lunar photometry, *Astrophys. J.*, **93**, 403–410, 1941.
- Moody, A., and A. H. Strahler, Characteristics of composited AVHRR data and problems in their classification, *Int. J. Remote Sens.*, **15**, 3473–3491, 1994.
- Nilson, T., and A. Kuusk, A reflectance model for the homogeneous plant canopy and its inversion, *Remote Sens. Environ.*, **27**, 157–167, 1989.
- Pinty, B., and M. M. Verstraete, Extracting information on surface properties from bidirectional reflectance measurements, *J. Geophys. Res.*, **96**, 2865–2874, 1991.
- Rahman, H., B. Pinty, and M. M. Verstraete, Coupled surface-atmosphere reflectance (CSAR) model, 2, Semiempirical surface model usable with NOAA advanced very high resolution radiometer data, *J. Geophys. Res.*, **98**, 20,791–20,801, 1993.
- Ross, J. K., *The Radiation Regime and Architecture of Plant Stands*, 392 pp., Dr. W. Junk Publishers, The Hague, 1981.
- Roujean, J. L., M. Leroy, and P. Y. Deschamps, A bidirectional reflectance model of the Earth's surface for the correction of remote sensing data, *J. Geophys. Res.*, **97**, 20,455–20,468, 1992.

- Strahler, A. H., Vegetation canopy reflectance modeling – recent developments and remote sensing perspectives, *Proc. 6th Int. Symp. Phys. Meas. Sign.*, 593–600, 1994.
- Strahler, A. H., and D. L. B. Jupp, Modeling bidirectional reflectance of forests and woodlands using Boolean models and geometric optics, *Remote Sens. Environ.*, 34, 153–166, 1990.
- Strahler, A. H., X. Li, S. Liang, J.-P. Muller, M. J. Barnsley, and P. Lewis, MODIS BRDF/Albedo product: Algorithm technical basis document, *NASA EOS-MODIS Doc.*, version 2.1, 55 pp., 1994.
- Strahler, A. H., M. J. Barnsley, R. d'Entremont, B. Hu, P. Lewis, X. Li, J.-P. Muller, C. B. Schaaf, W. Wanner, and B. Zhang, MODIS BRDF/Albedo product: Algorithm technical basis document, *NASA EOS MODIS Doc.*, version 3.2, 76 pp., 1995.
- Walthall, C. L., J. M. Norman, J. M. Welles, G. Campbell, and B. L. Blad, Simple equation to approximate the bidirectional reflectance from vegetation canopies and bare soil surfaces, *Appl. Opt.*, 24, 383–387, 1985.
- Wanner, W., A. H. Strahler, J.-P. Muller, M. Barnsley, P. Lewis, X. Li, and C. L. Barker Schaaf, Global mapping of bidirectional reflectance and albedo for the EOS MODIS project: the algorithm and the product, *Proc. Int. Geosci. Remote Sens. Symp. 95*, 525–529, 1995.
-
- X. Li, A. H. Strahler, and W. Wanner, Center for Remote Sensing, Boston University, 725 Commonwealth Avenue, Boston, MA 02215.
- (Received February 9, 1995; revised July 7, 1995; accepted July 7, 1995.)